J. Fluid Mech. (1993), *vol.* 250, *pp.* 531–551

Temperature dissipation in a turbulent round jet

By R. A. ANTONIA AND J. MI
Department of Mechanical Engineering, University of Newcastle, NSW, 2308, Australia

(Received 3 July 1992)

Parallel cold wires were used to measure the temperature derivative, in each of the three spatial directions, in the self-preserving region of a turbulent round jet. The temperature derivative variances were inferred from the correlation method and from the temperature derivative spectra after correcting these for the effect of wire separation. Both methods yielded fully consistent results for the components of the average temperature dissipation: the radial and azimuthal values are nearly equal and only slightly larger than the axial component. The resulting departure from isotropy of the temperature dissipation is small, especially when compared with results in other free shear flows. The high-wavenumber behaviour of the corrected temperature derivative spectra conforms closely with isotropy on the jet axis but small departures occur away from the axis. Conditional averages, based on spatially coherent temperature jumps, indicate that, while the organized motion makes a significant contribution to the temperature variance, its contribution to the temperature-derivative variances is small.

1. Introduction

Accurate estimates of the average temperature dissipation $\bar{\epsilon}_\theta = \alpha\overline{\theta_{,i}^2}$ ($\theta_{,i} \equiv \partial\theta/\partial x_i$, α is the thermal diffusivity, θ is the temperature fluctuation; unless otherwise mentioned, repeated subscripts imply summation) are needed to balance the budget of the temperature variance $\overline{\theta^2}$. They are also needed in engineering models which assume a constant value of the timescale ratio $(\overline{q^2}/\bar{\epsilon})/(\overline{\theta^2}/\bar{\epsilon}_\theta)$, where $\frac{1}{2}\overline{q^2}$ is the average turbulent kinetic energy and $\bar{\epsilon}$ is the average turbulent kinetic energy dissipation. More recently, $\overline{\theta^2}-\epsilon_\theta$ models with transport equations for $\overline{\theta^2}$ and $\bar{\epsilon}_\theta$ have been used in conjunction with a $k-\bar{\epsilon}$ model in different shear flows (e.g. Nagano & Kim 1988 in a boundary layer, Tulapurkara, Antonia & Browne 1989 in a wake). In turbulent combustion modelling, a knowledge of the joint probability density function between ϵ_θ and the scalar fluctuation θ is considered important for predicting turbulent diffusion flames (Bilger 1989).

The relative magnitudes of the three components of $\bar{\epsilon}_\theta$ can provide a measure of the departure from local isotropy. Measurements in a turbulent boundary layer by Krishnamoorthy & Antonia (1987) highlighted the strong anisotropy near the wall, a region dominated by $\overline{\theta_{,2}^2}$ (x_2 is in the direction normal to the wall). In the outer layer, the anisotropy was smaller but not negligible. The largest and smallest components were $\overline{\theta_{,3}^2}$ and $\overline{\theta_{,1}^2}$ (x_1 and x_3 are in the streamwise and spanwise directions respectively) as previously observed by Verollet (1972). Measurements of the three components of $\bar{\epsilon}_\theta$ in a quasi-homogeneous shear flow (Tavoularis & Corrsin 1981), a self-preserving plane jet (Antonia & Browne 1983) and a self-preserving plane wake (Antonia & Browne 1986), have also indicated significant departures from isotropy.

The situation in a circular jet appears to be different from that in the flows mentioned above. Using Raman-scattered light collected by a two-camera imaging system,

Namazian, Schefer & Kelly (1988) measured two components, $\alpha\overline{\theta^2_{,1}}$ and $\alpha\overline{\theta^2_{,2}}$ (in their experiment, θ is the fluctuating mass fraction of methane while α is the diffusivity of methane; x_2 is in the radial direction), of $\bar{\epsilon}_\theta$ in the developing region ($x_1/d \leqslant 17$) of an isothermal circular jet. At $x_1/d = 5$, $\overline{\theta^2_{,2}}$ was approximately equal to $\overline{\theta^2_{,1}}$ at the jet axis but increased relative to $\overline{\theta^2_1}$ away from the axis, the difference reaching a maximum near the half-radius. This difference decreased as x_1/d increased and was negligible at $x_1/d = 17$, apparently indicating that isotropy was achieved, provided the unmeasured azimuthal component $\overline{\theta^2_{,3}}$ is also equal to $\overline{\theta^2_{,2}}$ or $\overline{\theta^2_{,1}}$. Namazian *et al.*'s results at $x_1/d = 17$ are at variance with the earlier measurements by Lockwood & Moneib (1980), also in a circular jet, which indicated that $\overline{\theta^2_{,2}}$ was twice as large as $\overline{\theta^2_{,1}}$ on the axis at $x_1/d = 30$. The latter data, obtained with a pair of thermocouple wires (12.7 μm diameter) compensated for their thermal inertia, are likely to have suffered from the relatively large separation between the wires and the general difficulty of compensating for a fluctuating time constant. Hussein & George (1989) measured seven of the nine velocity derivatives that feature in the homogeneous expression for $\bar{\epsilon}$ in the self-preserving region of a circular jet. They found that the derivative data were in closer agreement with the assumption of local axisymmetry (signifying invariance of statistical properties with respect to a preferred direction†; The implications of this assumption were explored in more detail by George & Hussein 1991) than with local isotropy. As was noted by George & Hussein, the small-scale data in significant regions of the flows previously mentioned (e.g. boundary layer, plane jet, plane wake, homogeneous shear flow) also satisfy local axisymmetry more closely than local isotropy (see also Antonia *et al.* 1991). The axisymmetric values of $\bar{\epsilon}$ were significantly larger (by a factor of about 1.2 on the axis to about 2.3 at $x_2 \approx R_u$) than the isotropic estimates, thus suggesting a strong departure from isotropy. It should be noted however that a direct check of the accuracy of $\bar{\epsilon}$ via measurements of all the other terms in the transport equation is made difficult by the existence of the pressure diffusion term. For this reason, George & Hussein were not able to make a definitive statement on the accuracy of their axisymmetric distribution.

Since anisotropy may be more pronounced in $\bar{\epsilon}_\theta$ than $\bar{\epsilon}$ (e.g. the wake data of Browne, Antonia & Shah 1987), measurements of $\bar{\epsilon}_\theta$ may provide a sensitive indication of the anisotropy of a circular jet. Also, the accuracy of $\bar{\epsilon}_\theta$ can be checked with more confidence than $\bar{\epsilon}$ since the transport equation for $\overline{\theta^2}$ does not contain the pressure fluctuation. Two, not necessarily unrelated, characteristics make accurate turbulence measurements difficult in the circular jet. One of these is the presence of high turbulence intensity while the other is the occurrence of flow reversal in the outer region. In the present context, the first difficulty would need to be taken into account if Taylor's hypothesis were used for determining $\theta_{,1}$. In the present experiment, $\theta_{,1}$ was determined directly thus avoiding Taylor's hypothesis. The second difficulty was partially cirvumvented by taking most of the data in a region between the jet axis and the half-radius location, where flow reversal first becomes significant (Antonia, Chambers & Hussain 1980). A major challenge one faces when estimating $\theta_{,i}$ from a pair of parallel cold-wire signals is to establish that the values of $\overline{\theta^2_{,i}}$ are not adversely affected by the finite separation Δx_i between the cold wires. Although this problem has been discussed previously (for example, Browne, Antonia & Chambers 1983*a*; Brown, Antonia & Rajagopalan 1983*b*; Krishnamoorthy & Antonia 1987) it is readdressed in §4.

† These authors used x_1 as the preferred direction but noted (see also Antonia, Kim & Browne 1991) that other choices, e.g. the principal rate of strain direction, may be more suitable.

2. Experimental details

The jet was supplied by a variable centrifugal blower through an axisymmetric nozzle with a 10:1 contraction ratio. The air supply was heated by an electrical fan heater (2.4 kW) located at the blower entrance. At the nozzle exit (diameter d of 25.4 mm), the temperature T_j was 32 °C above ambient. In order to obtain a uniform and symmetrical (about the jet axis) mean temperature profile at the nozzle exit, the complete tunnel was insulated (25 mm thick insulating foam with a metallic foil overlay). At the nozzle exit, the temperature was uniform to within $\pm 1\%$.

Spatial derivatives of the temperature fluctuation θ were obtained using two parallel cold wires. Wollaston (Pt–10% Rh) wires of nominal diameter $d_w \approx 0.64$ μm were operated by in-house constant-current circuits supplying 0.1 mA to each wire. (For this current and the existing experimental conditions, the velocity contamination of the cold-wire signal was negligible for all the quantities considered in this paper.) The wires, with a nominal length l_w of about 0.45 mm, were perpendicular to the flow direction. Each wire was carefully checked under a microscope for straightness immediately prior to the experiments. Care was taken to ensure that the etched portion of each wire was central and parallel so as to minimize the uncertainty in the measurement of Δx_i, the separation in the x_i direction ($i = 1$, 2 and 3 stand for axial, radial and azimuthal directions respectively) between the wires.

The wires were mounted on separate traversing mechanisms, each fitted with a dial gauge with a least count of 0.01 mm. To determine the separation of Δx_i, each wire was separately brought into alignment with a fixed reference line (cross-hair of a cathetometer). When alignment was achieved, the dial gauges on the traversing mechanisms were set to zero. Estimates of the temperature coefficient of the cold wires were made by mounting the wires at the jet exit using a 10 Ω platinum resistance thermometer operated in a Leeds and Northrup 8087 bridge (with a resolution of 0.010 °C). Both wires and the associated electronic circuits were calibrated at the same time to minimize relative errors in wire calibrations.

Special attention was given to the choice of the wire length and the probe geometry to reduce the experimental error associated with the use of parallel wires for obtaining spatial derivatives. The diameter d_w (≈ 0.64 μm) and length l_w (≈ 0.45 mm) of the wires were chosen so that the ratio l_w/d_w (≈ 720) was sufficiently large to minimize possible attenuation at low wavenumbers (Paranthoen, Petit & Lecordier 1982) while keeping l_w/η, where $\eta \equiv (\nu^3/\bar{\epsilon})^{\frac{1}{4}}$ is the Kolmogorov microscale, as small as practicable. On the axis at $x_1/d = 30$, the experimental value of l_w/η (≈ 2.65) was small enough to minimize the attenuation at high wavenumbers (Wyngaard 1968). Only the central part of the Wollaston wires was etched to avoid difficulties associated with fully etched wires. For a given wire length, Paranthoen *et al.* (1982) found that the signal for a fully etched wire is more attenuated than that from a partially etched wire. The boundary-layer measurements of Anselmet *et al.* (1990) indicated that the r.m.s. temperature from a fully etched wire is significantly smaller than that for a partially etched wire.

In order to remove high-frequency electronic noise, the signals from both wires were first low-pass filtered. The filter settings were determined by viewing the time derivative spectra on the screen of a real-time spectrum analyser (HP3582A). Special attention was given to the degree of correlation between the two signals and to the time derivative spectra of these signals. If the spectra looked different, one or both of the wires were replaced by newly etched ones until no visible difference could be perceived. The correlation coefficient ρ between the two wires was higher than 0.994 for $\Delta x_i = 0.3$ mm at every location. The filter cutoff frequencies were identified with the

frequencies at which the derivative spectra were about 2–3 dB higher than the frequencies at which the noise first began to make a significant contribution. These settings were determined at each measurement location and found to be the same for the two wires. For the present experimental conditions, the filter cutoff frequency f_c was 2.2 kHz on the axis, where the Kolmogorov frequency f_K ($= \bar{U}/2\pi\eta$, $\bar{U}$ is the local mean velocity) was 2.0 kHz, and 1.2 kHz at $x_2 \approx R_u$, where f_K was about 0.8 kHz. The wires were cleaned in alcohol or re-etched to remove any contamination and then to avoid any possible degradation with time of the wire frequency response. According to Antonia, Browne & Chambers (1981), for $\bar{U} = 2$ m/s, the frequency response (-3 dB point) of a nominal 0.64 μm cold wire is about 2.5 kHz. It was therefore reasonable, as already noted by Tavoularis & Corrsin (1981), to neglect the possible effect on $\Delta\theta$ of unequal time constants of the two wires since the filter cutoff frequency was smaller than the frequency corresponding to the wire time constant.

After filtering, the signals from the two wires were passed through buck and gain units to offset the d.c. components and provide suitable amplification prior to digitizing the signals with a 12 bit A/D converter (RC Electronics) on a personal computer (NEC 386). The sampling frequency was chosen as twice the cutoff frequency and the record duration was 50 s. The digital data were directly transferred from the personal computer to a VAX 8550 computer using an ETHERNET (fibre-optic cable) link.

3. Experimental conditions

The jet exit velocity U_j was 11 m/s and the Reynolds number R_d ($\equiv U_j d/\nu$) was about 1.9×10^4. All measurements were made at $x_1/d = 30$ (for this flow, self-preservation was verified for $x_1/d \gtrsim 15$, Chua & Antonia 1986). On the axis, the mean velocity U_0 and mean temperature T_0 were 2.1 m/s and 4.8 °C (relative to ambient) respectively while $\overline{u_1^2}^{\frac{1}{2}}/U_0$ and $\overline{\theta^2}^{\frac{1}{2}}/T_0$ were 0.26 and 0.2 respectively. The turbulence Reynolds number $R_\lambda \equiv \overline{u_1^2}^{\frac{1}{2}}\lambda/\nu$ (where $\lambda = U_0^{-1}\overline{u_1^2}^{\frac{1}{2}}/\overline{u_{1,t}^2}^{\frac{1}{2}}$ and $u_{1,t} \equiv \partial u_1/\partial t$) was about 150. The Péclet number $P_\lambda \equiv \overline{u^2}^{\frac{1}{2}}\lambda_\theta/\alpha$, where $\lambda_\theta = \overline{\theta^2}^{\frac{1}{2}}/\overline{\theta_{,1}^2}^{\frac{1}{2}}$, was equal to 83. The half-radii R_u and R_θ, derived from mean velocity and mean temperature profiles respectively, were 75 mm and 90 mm. The ratio Gr/R_0^2 ($Gr \equiv gR_u^3 T_0/\nu T_a$ is the Grashof number where T_a is the absolute ambient temperature, and $R_0 \equiv U_0 R_u/\nu$ is the local Reynolds number) is about 0.0027, implying that buoyancy should be negligible and justifying the use of temperature as a passive contaminant. The Kolmogorov microscale η increases from about 0.17 mm on the axis to about 0.2 mm at $x_2 = R_u$.

4. Temperature-derivative variances

A possible way of determining $\overline{\theta_{,i}^2}$ (no summation on i here, $i = 1, 2, 3$ represent the axial, radial and azimuthal directions respectively) is to use the approximation

$$\theta_{,i} \approx \Delta\theta/\Delta x_i, \tag{1}$$

in the limit as $\Delta x_i^* \to 0$. There are however important random and systematic errors which arise in this process. The random errors include the uncertainties in measuring Δx_i and in determining the temperature coefficients of the cold wires. (As noted in §2, an effort was made to minimize both uncertainties.) The systematic error is most likely due to contamination by noise (both from the wires and the electronics). When Δx_i is very small, the signals from wires 1 and 2 may be assumed to be given by $(\theta + n_1)$ and $(\theta + n_2)$ respectively, where n_1 and n_2 are the uncorrelated noise contents of the two signals. The quantity $\overline{\theta_{,i}^2}$ will then systematically increase, approaching infinity as

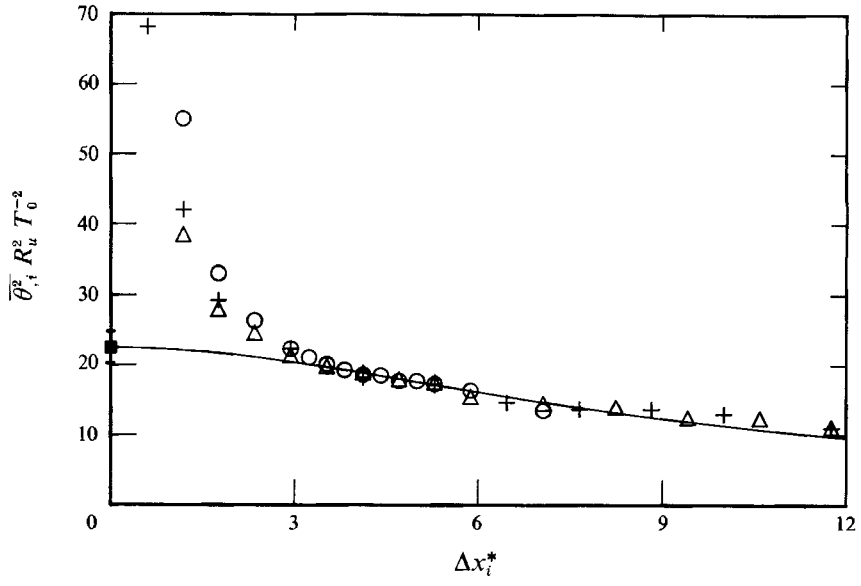

FIGURE 1. Mean-squared values of the measured $\theta_{,i}$ as a function of Δx_i^* on the jet axis: ○, $i = 1$; △, 2; +, 3; ■, $(\overline{\theta_{,i}^2})_{\text{corr}}$; ——, $r_i(\overline{\theta_{,i}^2})_{\text{corr}}$. I, error bar.

$\Delta x_i \to 0$ since $\overline{(\Delta\theta)^2}$ should approach a constant (non-zero) value $(\overline{n_1^2}+\overline{n_2^2})$. The increase is discernible on the $\overline{\theta_{,i}^2}$ data in figure 1 for $\Delta x_i^* \lesssim 3$ (see also Browne *et al.* 1983*a*, *b*). It is less pronounced in figure 2, where there is only one point below $\Delta x_i^* = 3$.

At very small Δx_i^* one would expect different $\overline{\theta_{,i}^2}$ corresponding to different i to converge to the same value, if the noise is the same in each case. In the present experiments, the cold wires often had to be replaced and the values of n_1 and n_2 are unlikely to have remained the same from one experiment to the next†. The location at which $\overline{\theta_{,i}^2}$ first rises is therefore difficult to define precisely. This and the increased importance of the random errors (Mestayer & Chambaud 1979) are good reasons to disregard data at small separations (say $\Delta x_i^* \lesssim 2$ or 3). Although correct in theory, Klewicki & Falco's (1990) prescription that Δx_i^* should be in the range $1.0 < \Delta x_i^* \leqslant 3.33$ and George & Hussein's (1991) suggestion that 'all of the spatial dimensions of the probes must be on the order of or smaller than the Kolmogorov microscale' may, in practice, lead to errors when selecting Δx_i^*. While it is conceivable that $\Delta x_i^* \approx 1$ may be adequate for some experimental conditions, such a choice should be made only after assessing (by experiment) the effect of varying Δx_i^*. For the data in figure 1, the use of $\Delta x_i^* \approx 1$ could result in $\overline{\theta_{,i}^2}$ being overestimated by as much as 170%.

It is not evident how one should infer the correct or true value of $\overline{\theta_{,i}^2}$ from the data of figure 1. An estimate of $\overline{\theta_{,i}^2}$ can also be obtained from the correlation $\overline{\theta(x_i)\,\theta(x_i+\Delta x_i)}$. With the assumption of homogeneity, the limiting behaviour (as $\Delta x_i \to 0$) of the correlation coefficient $\rho = \overline{\theta(x_i)\,\theta(x_i+\Delta x_i)}/\overline{\theta^2(x_i)}^{\frac{1}{2}}\overline{\theta^2(x_i+\Delta x_i)}^{\frac{1}{2}}$ is approximated by (Batchelor 1953)

$$\rho \approx 1-(\Delta x_i)^2/2\lambda_i^2, \tag{2}$$

where $\lambda_i = \overline{\theta^2}^{\frac{1}{2}}/\overline{\theta_{,i}^2}^{\frac{1}{2}}$ is the Taylor microscale for temperature. The assumption of

† The apparently faster increase for $i = 1$ than $i = 2$ or 3 (figure 2) may be due to probe interference effects when the wires are separated in the x_1 direction. We did check however that, at the first separation point, statistics of the temperature signal of the downstream wire did not change (within the experimental uncertainty) when the upstream wire was removed.

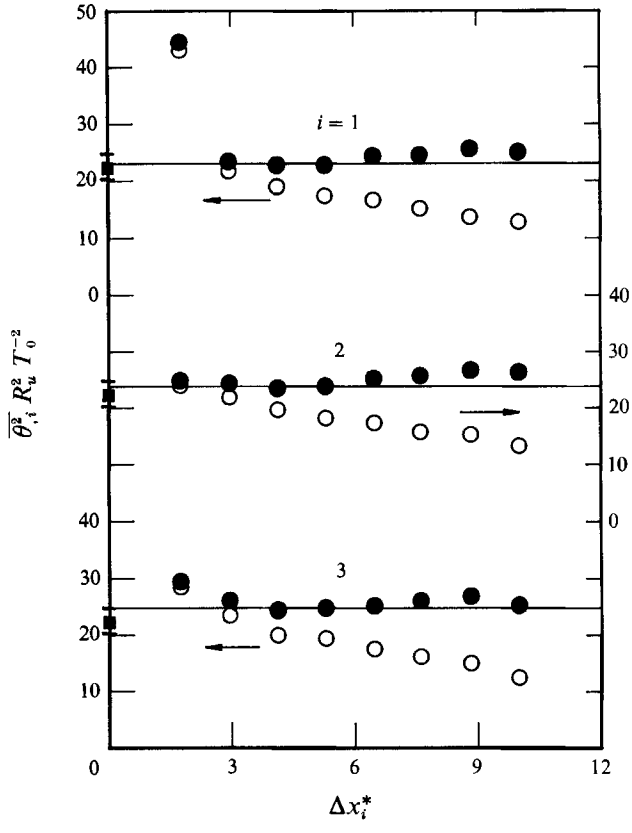

FIGURE 2. Mean-squared temperature derivative values on the jet axis. ○, uncorrected; ●, corrected; ■, correlation method. I, error bars. ——, $\overline{\theta^2_{,ic}}$ (average of corrected values in the range $3 \lesssim \Delta x_i^* \lesssim 6$).

homogeneity can be relaxed by including $(\overline{\theta^2})_{,i}$ in the Taylor series expansion of $\overline{\theta(x_i)\,\theta(x_i+\Delta x_i)}$. The resulting expression for ρ, which is similar to that given in Townsend (1956) for the velocity correlation, is

$$\rho = 1 - \tfrac{1}{2}(\Delta x_i)^2 \left\{ \frac{\overline{\theta^2_{,i}}}{\overline{\theta^2}} - \frac{[(\overline{\theta^2})_{,i}]^2}{4\overline{\theta^2}^2} \right\}. \tag{3}$$

The main non-homogeneity is in the x_2 direction. However, the maximum value of the ratio of the second and first terms inside the braces in (3) is about 0.003 for $i = 2$ (at $x_1/d = 30$), suggesting that (2) should be adequate for all i.

The value of λ_i is usually inferred from a log–log plot of $(1-\rho)$ *vs.* Δx_i^* at small Δx_i^*. Such a plot should, for consistency with (2), indicate a linear behaviour, with a slope of $+2$, as $\Delta x_i^* \to 0$. There is a small Δx_i^* range in figure 3 where (2) is satisfied but there is a noticeable departure at the smallest Δx_i^* (the data of Rose 1966 and Champagne, Harris & Corrsin 1970, show the same trend – which these authors attributed to probe interference effects and electronic noise; the accuracy of their velocity Taylor microscales was estimated to be $\pm 5\%$). The correlation values of $\overline{\theta^2_{,i}}$, hereafter referred to as $(\overline{\theta^2_{,i}})_{\mathrm{corr}}$, are shown on the ordinates of figures 1 and 2. They are nearly independent of i at all ξ ($\equiv x_2/R_u$), implying that the isotropic relation

$$\overline{\theta^2_{,1}} = \overline{\theta^2_{,2}} = \overline{\theta^2_{,3}} \tag{4}$$

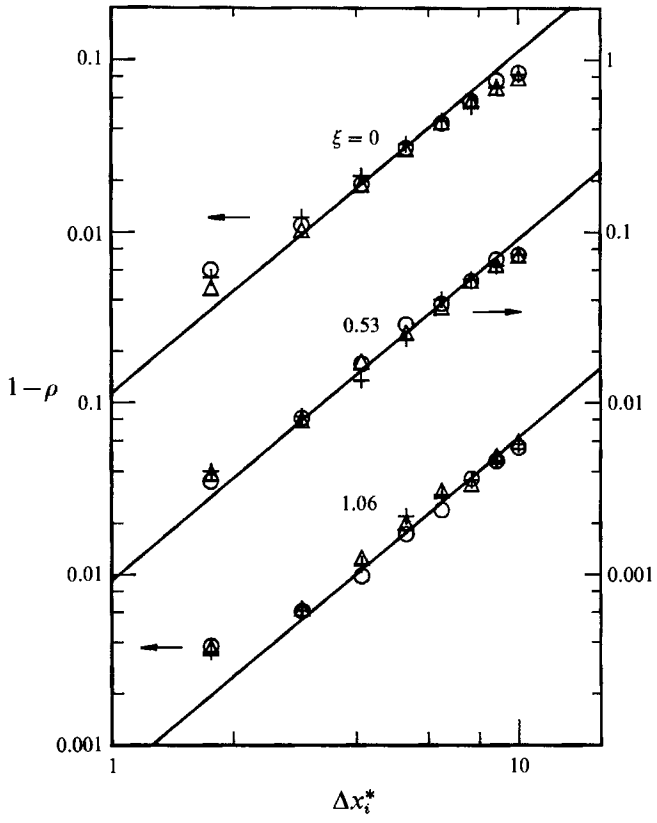

FIGURE 3. Log-log representation of $(1-\rho)$ as a function of Δx_i^* at three flow locations. ○, $i = 1$; △, 2; +, 3. ——, lines of slope of +2.

is nearly approximated by the data. The collapse of the data in figure 3 suggests that, for the same value of Δx_i,

$$\rho(\Delta x_1) = \rho(\Delta x_2) = \rho(\Delta x_3) \tag{5}$$

is also nearly approximated by the data. Like (4), (5) is consistent with local isotropy (e.g. Monin & Yaglom 1975, p. 136; Mestayer 1982). The $(1-\rho)$ data of figure 3 differ significantly from the corresponding data in the wake (Antonia & Browne 1986, figure 5) and the boundary layer (figure 2 of Krishnamoorthy & Antonia 1987), the departure from (4) and (5) being significantly larger in the latter two flows.

Wyngaard's (1971) analysis provides a way of estimating the effect of Δx_i on the measured values of $\overline{\theta_i^2}$, through equation (1). The adaptation of Wyngaard's analysis to spatial temperature derivatives was presented in Browne *et al.* (1983*b*); it allows the high-wavenumber part of the $\theta_{,i}$ spectrum to be corrected for the effect of Δx_i. The spectrum of $\theta_{,i}$, is given by (cf. the Appendix)

$$\phi_{\theta_{,i}}(k_1, \Delta x_i) = \frac{4}{(\Delta x_i)^2} \int\int_{-\infty}^{\infty} \sin^2\left(\frac{k_i \Delta x_i}{2}\right) \phi(k)\, \mathrm{d}k_2\, \mathrm{d}k_3, \tag{6}$$

where k is the magnitude $(k_1^2+k_2^2+k_3^2)^{\frac{1}{2}}$ of the wavenumber vector $\boldsymbol{k}$ and $\phi(k)$ is related to the three-dimensional spectrum $\Gamma(k)$ by

$$\phi(k) = \Gamma(k)/4\pi k^2. \tag{7}$$

Although the analysis which leads to (6) assumes isotropy, its purpose is to correct the attenuation of the high-wavenumber part of $\phi_{\theta,i}$ due to Δx_i. In this sense, the application of the analysis to the present data should not therefore force agreement with (4) since one would expect departures from isotropy to reside mainly at low wavenumbers. $\Gamma(k)$ can be estimated from the one-dimensional temperature spectrum $\phi_\theta(k_1)$ by the isotropic relation

$$\Gamma(k) = -k(\partial\phi_\theta/\partial k_1)_{k_1=k}. \tag{8}$$

The measured $\phi_{\theta,i}$ can be corrected by multiplying it with the factor

$$R_i \equiv \phi_{\theta,i}(k_1, \Delta x_i \to 0)/\phi_{\theta,i}(k_1, \Delta x_i)$$

inferred from (6). For $i = 1$,

$$R_1 = \tfrac{1}{4}(k_1 \Delta x_1)^2 \sin^{-2}(\tfrac{1}{2}k_1 \Delta x_1). \tag{9}$$

This correction is independent of $\Gamma(k)$. It is also independent of isotropy since it can be obtained from (A 3) and (A 4) of the Appendix. For $i = 2$ or 3,

$$R_2 = R_3 = \tfrac{1}{4}(\Delta x_i)^2 \frac{\int\int_{-\infty}^{\infty} k_i^2 \dfrac{\Gamma(k)}{4\pi k^2}\,\mathrm{d}k_2\,\mathrm{d}k_3}{\int\int_{-\infty}^{\infty} \sin^2(\tfrac{1}{2}k_i \Delta x_i)\dfrac{\Gamma(k)}{4\pi k^2}\,\mathrm{d}k_2\,\mathrm{d}k_3}. \tag{10}$$

The integration in (6) was carried out numerically, after $\Gamma(k)$ was determined from (8), at each measurement location. Measured spectra of $\theta_{,i}$ at the jet axis are shown in figure 4 in terms of the normalized wavenumber k_1^* ($\equiv k_1\eta$). The corrected spectra, using (9) and (10), are also shown in this figure, the normalization being such that

$$\int_0^\infty \phi^*_{\theta,i}(k_1^*)\,\mathrm{d}k_1^* = \overline{\theta^2_{,i}}(\eta/\theta_K)^2$$

(θ_K is the Kolmogorov temperature scale). As $k_1^* \to 1$, the measured spectra show the expected attenuation at high wavenumbers as Δx_i increases (the arrows are in the direction of increasing Δx_i^*). All three sets of corrected spectra collapse, allowing for the experimental uncertainty, at nearly all values of k_1^*. This collapse implies unique values of $\overline{\theta^2_{,i}}(\eta/\theta_K)^2$, perhaps with a larger uncertainty for $i = 1$ than $i = 2$ or 3. These values were obtained by multiplying the measured values of $\overline{\theta^2_{,i}}$ by r_i, where

$$r_i \equiv \frac{\int_{-\infty}^{\infty} \phi_{\theta,i}(k_1)\,\mathrm{d}k_1}{\int_{-\infty}^{\infty} R_i^{-1}\phi_{\theta,i}(k_1)\,\mathrm{d}k_1}. \tag{11}$$

The distribution of $r_i(\overline{\theta^2_{,i}})_{\mathrm{corr}}$ shown in figure 1 is consistent with the data in the range $3 \lesssim \Delta x_i^* \lesssim 9$, suggesting that the Wyngaard-based correction is adequate in the present flow. Figure 2 shows that when r_i is applied to each data point, there is a range of Δx_i^* in which the corrected value of $\overline{\theta^2_{,i}}$, denoted by $\overline{\theta^2_{,ic}}$, is nearly constant. The difference between $\overline{\theta^2_{,ic}}$ and $(\overline{\theta^2_{,i}})_{\mathrm{corr}}$ is small (the uncertainty in $\overline{\theta^2_{,ic}}$ is slightly smaller than that in $(\overline{\theta^2_{,i}})_{\mathrm{corr}}$ so that the former estimates are used in § 5).

Although Taylor's hypothesis is not used here, it is of interest to note that on the jet axis, $\overline{\theta^2_{,ic}}$ is in reasonable agreement with the value that would be obtained from the relation $\overline{\theta^2_{,1}} = \bar{U}^{-2}(\overline{\partial\theta/\partial t})^2$. However, this relation becomes increasingly inaccurate as

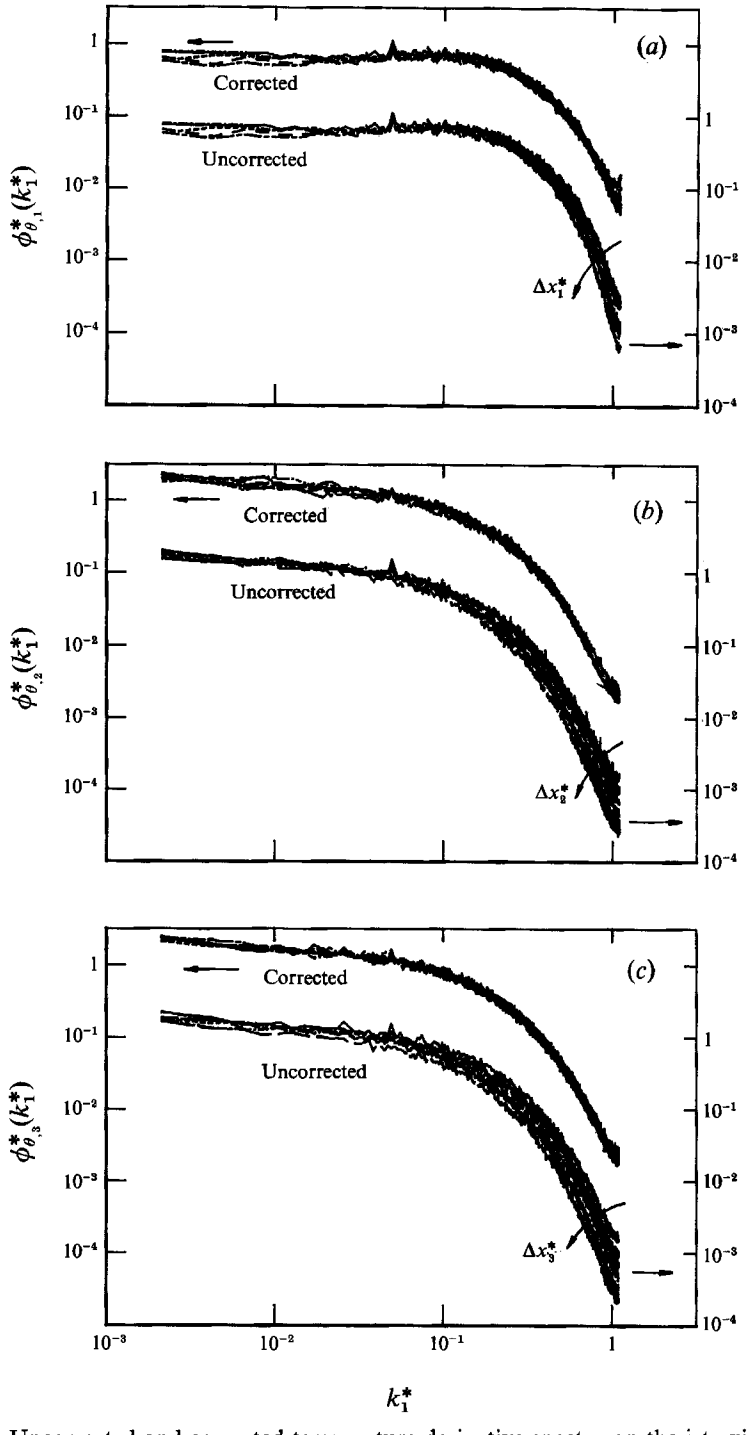

FIGURE 4. Uncorrected and corrected temperature derivative spectra on the jet axis. (Arrows are in direction of increasing separation between cold wires.) (*a*) $\theta_{,1}$ (Δx_1^* in the range 2.3 to 4.7); (*b*) $\theta_{,2}$ (Δx_2^* in the range 2.9 to 10); (*c*) $\theta_{,3}$ (Δx_3^* in the range 2.9 to 10).

the distance from the axis increases; the Lumley (1965)-based Wyngaard–Clifford (1977) correction to Taylor's hypothesis (see also George, Hussein & Woodward 1989) appears to represent the present values of $\overline{\theta^2_{,1c}}$ well (a detailed comparison between the statistics of temporal and streamwise derivatives will be presented elsewhere).

5. Temperature dissipation and $\overline{\theta^2}$ budget

Distributions across the jet of the average temperature dissipation and of its three components are shown in figure 5. The azimuthal and radial components of $\bar{\epsilon}_\theta$ are approximately equal everywhere in the flow. The equality $\overline{\theta^2_{,2}} = \overline{\theta^2_{,3}}$ is expected on the jet axis as a consequence of symmetry. Away from the axis, the validation of this equality by the present data indicates support for local axisymmetry or rotational symmetry about x_1. George & Hussein (1991) show (their table 3) that the equality $\overline{\theta^2_{,2}} = \overline{\theta^2_{,3}}$ is reasonably well supported by data in different shear flows. In the present flow, the magnitude of $\overline{\theta^2_{,1}}$ is only slightly smaller than that of the other two components so that the departure from local isotropy appears to be small. The present results support and extend those of Namazian *et al.* (1988) but appear to be at variance with the strong anisotropy of the velocity derivatives reported by George & Hussein (1991).

A measure of the departure from local isotropy is given by the ratio $\bar{\epsilon}_\theta/(\bar{\epsilon}_\theta)_{\rm iso}$. Figure 6 shows that the ratio is nearly equal to 1 on the axis and increases only slightly across the jet. This behaviour contrasts strongly with that in a plane jet and in a plane wake. Values of this ratio obtained from Antonia & Browne (1983) for the plane jet and from Browne *et al.* (1987) for the wake are also shown in figure 6.

An indirect validation of the measured values of $\bar{\epsilon}_\theta$ is provided by the budget of $\frac{1}{2}\overline{\theta^2}$. After neglecting the viscous diffusion term, an approximate form of this budget is given by

$$\underbrace{\bar{U}\frac{\partial \frac{1}{2}\overline{\theta^2}}{\partial x_1} + \bar{V}\frac{\partial \frac{1}{2}\overline{\theta^2}}{\partial x_2}}_{\text{Advection}} + \underbrace{\frac{x_2^{-1}}{2}\frac{\partial}{\partial x_2}(x_2\overline{v\theta^2})}_{\text{Diffusion}} \underbrace{+\overline{v\theta}\frac{\partial \bar{T}}{\partial x_2}}_{\text{Production}} + \underbrace{\bar{\epsilon}_\theta}_{\text{Dissipation}} = 0. \tag{12}$$

Estimates of the advection and production terms were based on the assumption of self-preservation. In particular, $\bar{U}$, $\bar{T}$ and $\overline{\theta^2}$ are given by

$$\bar{U} = U_0 f_1(\xi), \quad \bar{T} = T_0 f_2(\xi), \quad \overline{\theta^2} = T_0^2 f_3(\xi). \tag{13}$$

Expressions (13) were closely supported by Chua's (1989) measurements, the axial variations of R_u, U_0 and T_0 being given by

$$R_u/d = 0.099(x_1/d - 0.027),$$
$$U_0/U_j = [0.18(x_1/d - 0.8)]^{-1},$$
$$T_0/T_j = [0.23(x_1/d - 1)]^{-1}.$$

The radial velocity $\bar{V}$ was calculated using the continuity equation

$$\frac{\partial \bar{U}}{\partial x_1} + x_2^{-1}\frac{\partial (x_2 \bar{V})}{\partial x_2} = 0,$$

while the radial heat flux $\overline{v\theta}$ was inferred from Chua's (1989) measurements of $\overline{v\theta}$ in the self-preserving flow region.

The terms on the left-hand side of (12) are plotted in figure 7 after normalization by

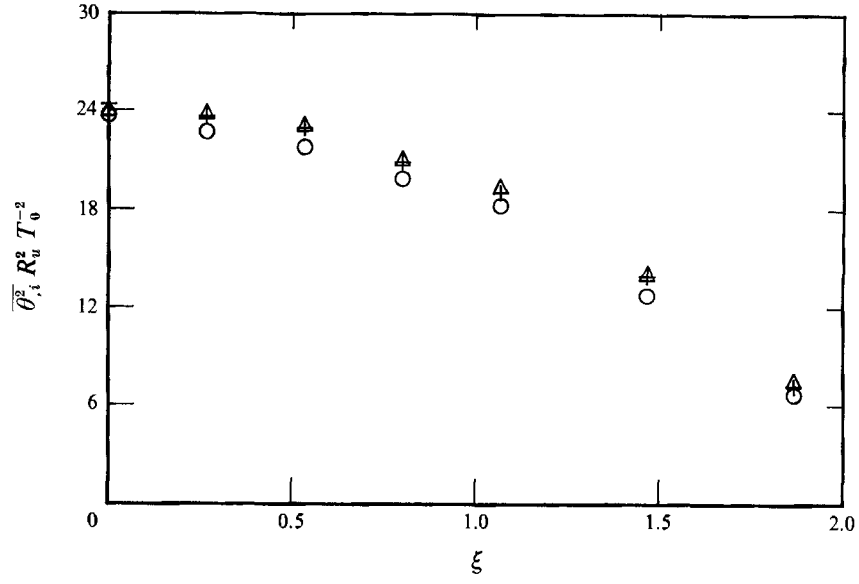

FIGURE 5. Corrected components of the temperature dissipation: ○, $i = 1$; △, 2; +, 3.

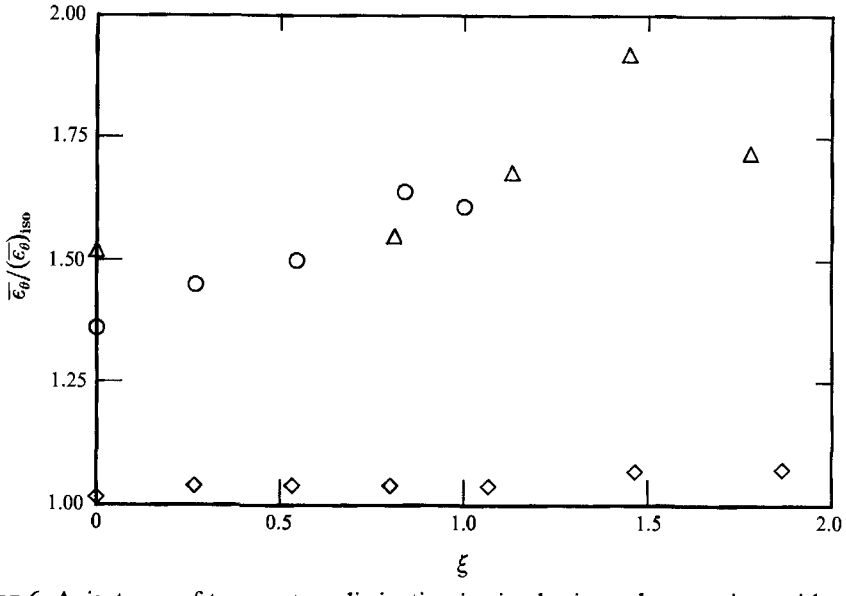

FIGURE 6. Anisotropy of temperature dissipation in circular jet and comparison with plane jet and plane wake: ◇, present; ○, plane jet (Antonia & Browne 1983); △, plane wake (Browne *et al.* 1987).

$U_0 T_0^2 R_u^{-1}$. The diffusion term was not measured; it was only inferred by difference. The variation of this term across the jet is reasonable since the positive and negative areas under the diffusion curve are approximately equal, consistent with the requirement

$$\int_0^\infty \tfrac{1}{2} x_2^{-1} \frac{\partial}{\partial x_2} (x_2 \overline{v\theta^2})\, \mathrm{d}x_2 = 0.$$

The diffusion is very similar to that measured by Antonia, Prabhu & Stephenson (1975) in a round jet with a co-flowing stream.

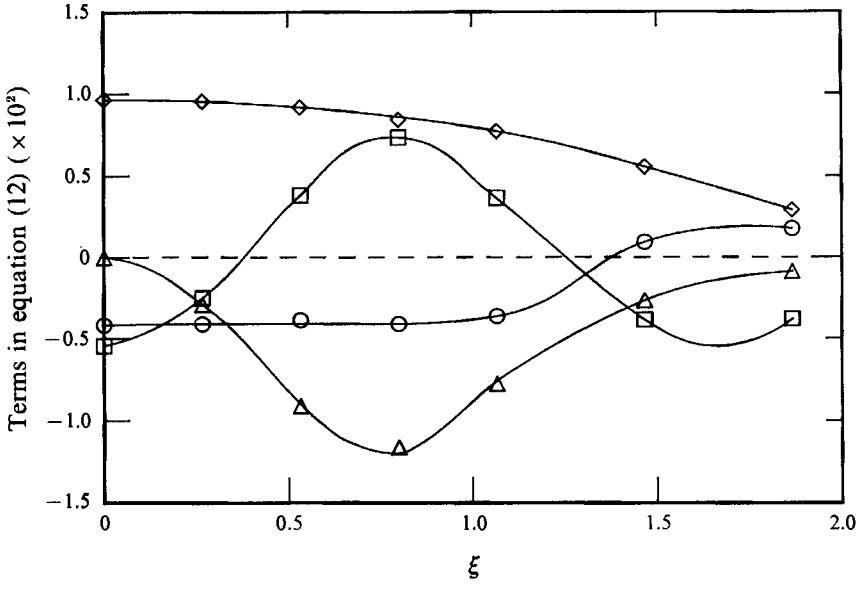

FIGURE 7. Measured budget of $\frac{1}{2}\overline{\theta^2}$: △, production; ○, advection; ◇, dissipation; □, diffusion (by difference).

The magnitude of $\bar{\epsilon}_\theta$ decreases only slightly between the axis and $\xi \approx 1$, i.e. a region for which the flow is approximately fully turbulent (the intermittency factor is about 0.98 at $\xi = 1$; Chua 1989; Wygnanski & Fiedler 1969). It should be noted that the budget in figure 7 is very similar to that given in Antonia *et al.* (1975). Since local isotropy was used in the latter paper to estimate $\bar{\epsilon}_\theta$ (the resulting imbalance in the budget was small), the present results provide an important verification of this assumption.

6. Contributions from temperature jumps to temperature-derivative variances

The ramp-like temperature signature in a circular jet and various other shear flows has been observed by several authors (see Broadwell & Mungal 1991, for references). This signature is characterized by a relatively sudden increase or jump in temperature which is followed by a gradual decrease. Antonia *et al.* (1975) and Sreenivasan, Antonia & Britz (1979) noted that the jump is coherent over a significant part of the jet. Sreenivasan (1991) drew attention to the similarity between the ramp-like occurrences in the concentration field and the highly dissipative three-dimensional sheet-like structures inferred from two-dimensional images (obtained by a laser-induced fluorescence technique) of a circular jet. Away from the jet axis, the sheets have a preferred orientation (about 45°), which corresponds to that of the principal axis for mean strain (see also Van Cruyningen, Lozano & Hanson 1990). This evidence led Sreenivasan to suggest that isotropy is neither 'natural' nor 'obvious' for the small-scale scalar field. The present near-equality of the three temperature-derivative variances in apparent conformity with isotropy, suggests that it would be useful to quantify the contributions to these variances from the sheet-like structures. As no attempt was made in the present investigation to identify these sheet-like structures, we restrict our attention to the temperature jumps and attempt to estimate their contributions to the temperature derivative variances.

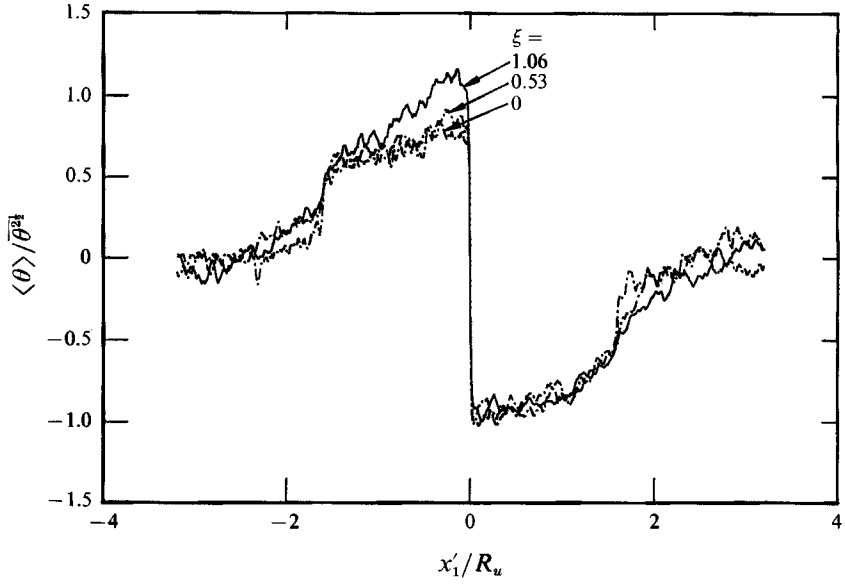

FIGURE 8. Averages of θ conditioned on temperature jumps at $\xi = 0$, 0.53 and 1.06.

The jumps are detected here with the WAG (window average gradient) method (Antonia & Fulachier 1989; Bisset, Antonia & Browne 1990). For each point in the digital-temperature time series, θ_j, the quantity

$$\mathrm{WAG}_j = \frac{1}{2\tau}\left(\sum_{m=j+1}^{j+\tau} \theta_m - \sum_{m=j-\tau}^{j-1} \theta_m \right)$$

is calculated. A detection region begins when WAG_j first exceeds $k\overline{\theta^2}^{\frac{1}{2}}$, where k is a threshold, and ends when WAG_j becomes negative. Each detection point d_i is the instant at which WAG_j is largest within a detection region. The detection window length $2\tau+1$ and the threshold were chosen equal to the number of the θ_m points covering a half of the average period of the organized motion in its time series (for example, 500 at the axis) and 0.5, respectively. This choice was made such that the number of detections obtained was approximately equal to that of the whole sampling duration (= 50 s) multiplying with the average frequency f_1 of the organized motion.

The temperature fluctuation θ is decomposed into $\langle\theta\rangle$, the component of θ associated with the detected organized motion, and θ_r, the remainder, namely

$$\theta = \langle\theta\rangle + \theta_r. \tag{14}$$

The coherent component is given by

$$\langle\theta\rangle = \frac{1}{N}\sum_{i=1}^{N} \theta(d_i + t), \tag{15}$$

where N is the total number of detections and t is time measured relative to d_i. Distributions of $\langle\theta\rangle/\overline{\theta^2}^{\frac{1}{2}}$ at $\xi = 0$, 0.53 and 1.06 are shown in figure 8 in terms of $x'_i \equiv -tU_c$, where U_c is the convection velocity of the organized motion. U_c was inferred from temperature space–time correlations (using two cold wires separated in the axial direction). The magnitude of U_c decreased between $0.99\,U_0$ on the axis and $0.72\,U_0$ at the half-radius. Conditional averages in figure 8 indicate a jump in $\langle\theta\rangle$ near $x'_1 = 0$. The magnitude of the jump increases as ξ increases (such an increase was also observed in a plane jet, Antonia *et al.* 1986).

ξ	$\overline{\overline{\langle\theta\rangle^2}}/\overline{\theta^2}$	$\overline{\overline{\langle\theta\rangle_{,1}^2}}/\overline{\theta_1^2}$	$\overline{\overline{\langle\theta\rangle_{,2}^2}}/\overline{\theta_2^2}$	$\overline{\overline{\langle\theta\rangle_{,3}^2}}/\overline{\theta_3^2}$
0	26.5	4.8	0.8	0.9
0.27	27.3	5.2	0.9	1.1
0.53	30.4	6.4	1.3	1.2
0.80	33.2	7.8	2.1	1.4
1.06	35.6	8.7	2.9	1.8

TABLE 1. Estimates, as percentages, of contributions from detected motion to $\overline{\theta^2}$ and $\overline{\theta_{,i}^2}$

To help quantify the contributions from the detection motion to $\overline{\theta^2}$ and $\overline{\theta_{,i}^2}$, structural averages are introduced, viz.

$$\overline{\overline{\langle f\rangle^n} = \frac{1}{t_2-t_1}\int_{t_1}^{t_2}\langle f(t)\rangle^n \,\mathrm{d}t, \tag{16}}$$

where f represents either θ or $\theta_{,i}$. The times t_1 and t_2 (relative to the detection) were selected so that $t_1 U_c = -\frac{1}{2}\Lambda$ and $t_2 U_c = +\frac{1}{2}\Lambda$, where Λ is the wavelength of the organized motion. Chua's (1989) space–time correlations of the longitudinal velocity fluctuation at $x/d = 30$ were used for selecting Λ ($\approx 6.4\,R_u$). This value is in reasonable agreement with that ($\approx 6\,R_u$) of Tso, Kovasznay & Hussain (1981), also for a circular jet ($40 \leqslant x/d \leqslant 50$). The average frequency f_1 of the organized motion may be defined by $f_1 = U_c/\Lambda$. The present values of $f_1 R_u/U_0$ are in the range 0.15 ($\xi = 0$) to 0.11 ($\xi \approx 1$). Interestingly, these values compare favourably with the average frequency (≈ 0.11 non-dimensionalized on U_0 and the half-width L_u) of the organized motion in a plane jet (e.g. Cervantes de Gortari & Goldschmidt 1981; Antonia *et al.* 1983).

After differentiating (14) with respect to x_i (and noting that $\langle\theta\rangle_{,i} \equiv \langle\theta_{,i}\rangle$), squaring, and structurally averaging, we have

$$\overline{\overline{\langle\theta_{,i}^2\rangle} = \overline{\overline{\langle\theta\rangle_{,i}^2} + \overline{\overline{\langle\theta_{r,i}^2\rangle}},}$$

where $\overline{\overline{\langle\theta_{,i}^2\rangle}} \equiv \overline{\theta_{,i}^2}$. The ratios $\overline{\overline{\langle\theta\rangle_{,i}^2}}/\overline{\theta_{,i}^2}$ are shown in table 1 together with $\overline{\overline{\langle\theta\rangle^2}}/\overline{\theta^2}$, the contribution of the detected motion to the temperature variance. While the latter contribution is significant (ranging between 26.5% at $\xi = 0$ and 35.6% at $\xi \approx 1$), the contributions to the derivative variances are quite small on the axis, increasing only slightly to the half-radius location. This reflects the previously noted increase of $\langle\theta\rangle$ with respect to ξ, near $x' = 0$ (figure 8). Although the tabulated values of $\overline{\overline{\langle\theta\rangle_{,i}^2}}$ were obtained for $\Delta x_i^* \approx 5.3$, we have verified that the values are practically unchanged for $3 \lesssim \Delta x_i^* \leqslant 10$. The sensitivity of the temperature jump results to the detection process was checked by varying the detection window length ($2\tau + 1$) and the threshold (k); the variation affected $\overline{\overline{\langle\theta\rangle_{,i}^2}}$ by less than 10%.

The table indicates that the contribution of the detected motion to the streamwise-derivative variance is slightly larger than to either the x_2 or x_3 derivative variances. Since $\overline{\theta_{,1}^2}$ is somewhat smaller than $\overline{\theta_{,2}^2}$ (or $\overline{\theta_{,3}^2}$), the tabulated values indirectly suggest that the remainder motion contributes more to $\overline{\theta_{,2}^2}$ (or $\overline{\theta_{,3}^2}$) than to $\overline{\theta_{,1}^2}$. However, this does not imply that the random part of $\overline{\theta_{,i}^2}$ is more anisotropic than $\overline{\theta_{,i}^2}$ itself, since the detection scheme does not capture all the coherent structures.

The temperature jumps, which are convected in the flow direction, may be skewed or curved in the lateral directions. It would be reasonable to expect large values of $\theta_{,i}^2$ (though not necessarily simultaneously) to be associated with the jumps. To quantify

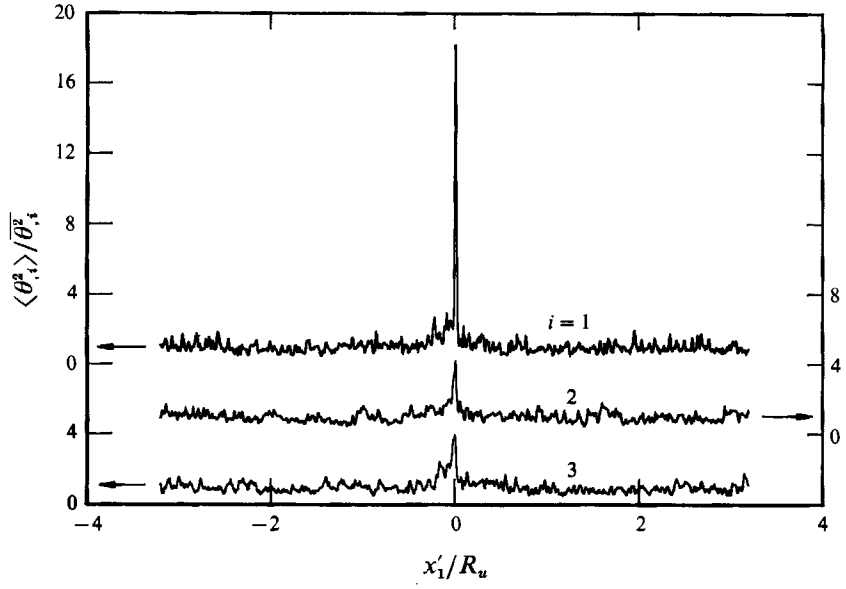

FIGURE 9. Averages of $\theta^2_{,i}$ conditioned on temperature jumps at $\xi = 0$.

this expectation, conditional averages of $\theta^2_{,i}$ were formed, using the following relation, similar to (15):

$$\langle\theta^2_{,i}\rangle = \frac{1}{N}\sum_{i=1}^{N}\theta^2_{,i}(d_i + t).$$

The resulting distributions on the axis (figure 9) indicate good coincidence between the jumps and the activity in $\theta^2_{,i}$. There is also strong activity in these quantities immediately after the jump occurs. Most of the activity is, however, concentrated in a very narrow region near $x_1' = 0$, with the largest peaks at negative values of x_1'/R_u. The peak in $\langle\theta^2_{,1}\rangle$ is much larger than in $\langle\theta^2_{,2}\rangle$ or $\langle\theta^2_{,3}\rangle$. A possible reason for this is that the normal to the curved surfaces of the jumps is, on average, aligned mostly in the x_1 direction so that the absolute value of the streamwise component of the temperature gradient should be larger than that in the two lateral directions.

7. Temperature-derivative spectra: comparison with isotropy

The measured (corrected) spectra of $\theta_{,i}$ are plotted in figure 10 as a function of the normalized one-dimensional wavenumber k_1^* ($= k_1\eta$) for three values of ξ ($= 0$, 0.53 and 1.06). The near equality of $\phi_{\theta_{,2}}$ and $\phi_{\theta_{,3}}$ is consistent with that previously observed in other flows: for example a plane jet (Antonia & Browne 1983) and a boundary layer (Sreenivasan *et al.* 1977). Relative to $\phi_{\theta_{,1}}$, $\phi_{\theta_{,2}}$ and $\phi_{\theta_{,3}}$ are larger at low wavenumbers and lower at high wavenumbers. On the axis, $\phi_{\theta_{,1}}$ monotonically increases for $k_1^* \lesssim 0.1$ while, away from the axis, there is a monotonic decrease with k_1^* over the same wavenumber range. This decrease is slightly more accentuated at $\xi = 1.06$ (figure 10*c*) than at $\xi = 0.53$ (figure 10*b*). This behaviour appears consistent with the slight increase in the values of $\overline{\langle\theta\rangle^2_{,1}}/\overline{\theta^2_{,1}}$ as ξ increases.

Also shown in figure 10 are the calculated distributions of $\phi_{\theta_{,2}}$ and $\phi_{\theta_{,3}}$ using the isotropic relation (Van Atta 1977)

$$\phi_{\theta_{,2}}(k_1) = \phi_{\theta_{,3}}(k_1) = \int_{k_1}^{\infty} k^{-1}\phi_{\theta_{,1}}(k)\,\mathrm{d}k \qquad (17)$$

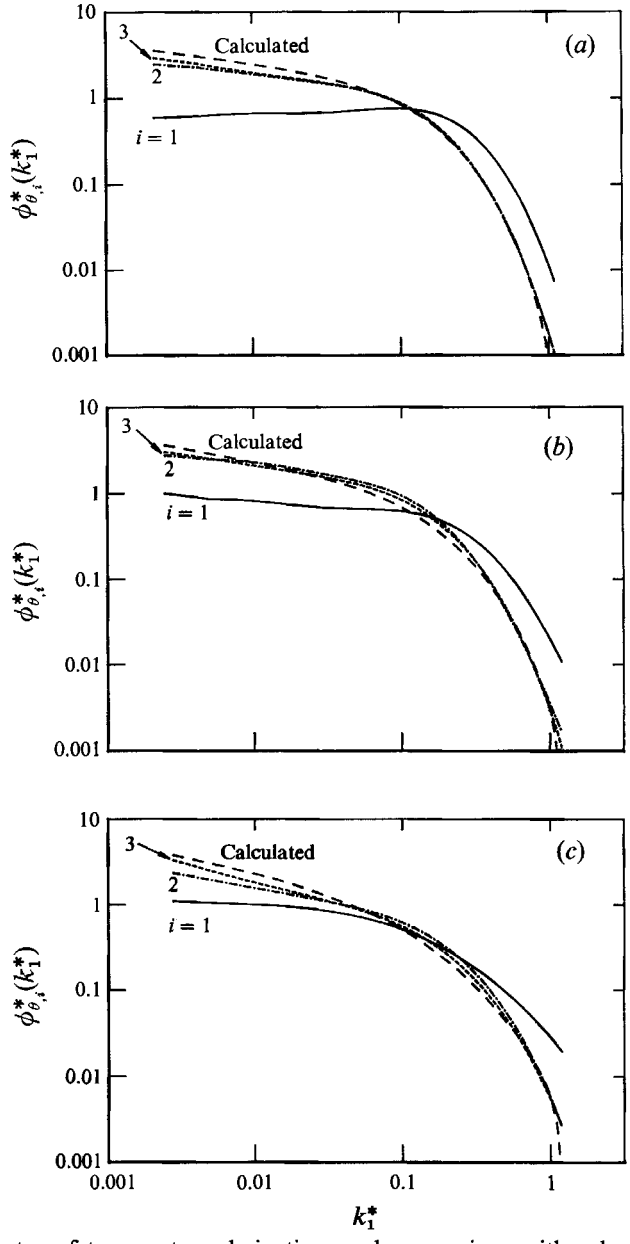

FIGURE 10. Spectra of temperature derivatives and comparison with calculations, based on local isotropy. Measured: ——, $\phi^*_{\theta,1}$; — — —, $\phi^*_{\theta,2}$; ----, $\phi^*_{\theta,3}$. Calculated: ——, $\phi^*_{\theta,2}$ or $\phi^*_{\theta,3}$. (*a*) $\xi = 0$; (*b*) 0.53; (*c*) 1.06.

and the measured (corrected) values of $\phi_{\theta,1}$. (Before carrying out the integration in (17), a high-order polynomial fit was applied to the data for $\ln \phi_{\theta,1}$ *vs.* $\ln k_1$.)

On the axis of the jet, the calculated and measured (corrected) spectra of $\theta_{,2}$ and $\theta_{,3}$ are in excellent agreement with each other for $k_1^* \gtrsim 0.05$. For $k_1^* < 0.05$, the calculations are slightly above the measurements, apparently reflecting a small degree of low-wavenumber anisotropy. This anisotropy is however much smaller than that previously obtained on the centreline of a plane jet (Antonia, Browne & Chambers 1985). At $\xi = 0.53$ and 1.06, the agreement between measurement and calculation is

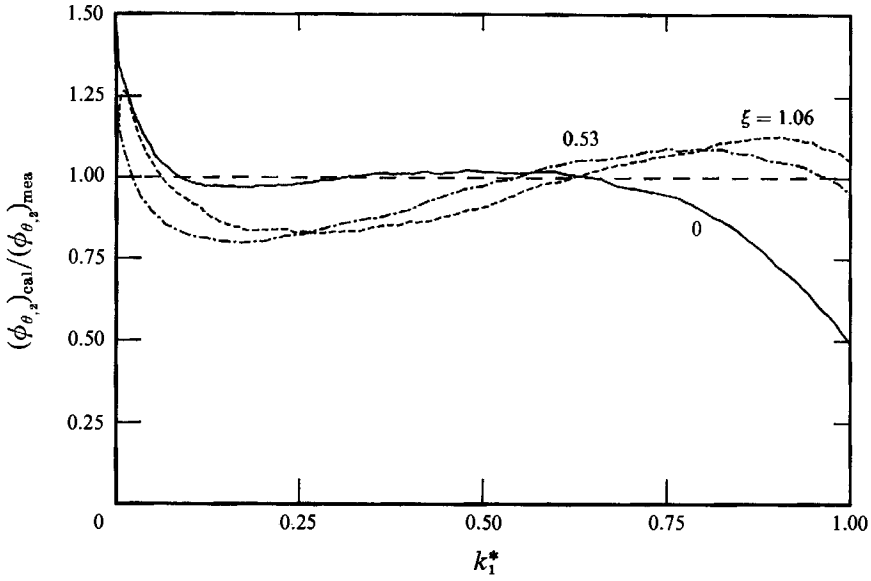

FIGURE 11. Ratio of measured and calculated spectra of $\theta_{,2}$ at $\xi = 0$, 0.53 and 1.06: ——, $\xi = 0$; —·—, 0.53; ----, 1.06.

not as good as at $\xi = 0$, reflecting the difference between $\overline{\theta_{,2}^2}$ (or $\overline{\theta_{,3}^2}$) and $\overline{\theta_{,1}^2}$ as ξ increases.

While figure 10 apparently indicates that the departure from isotropy is small when k_1^* is sufficiently large, the use of a logarithmic scale tends to minimize departures between the measured and calculated spectra of $\theta_{,2}$ (or $\theta_{,3}$). To emphasize such departures, the ratio $(\phi_{\theta,2})_{cal}/(\phi_{\theta,2})_{mea}$ is plotted in figure 11 on a linear scale. At $\xi = 0.53$ and 1.06, this ratio is in the range 0.80 to 1.10 for $k_1^* \gtrsim 0.05$. On the axis, the ratio is nearly 1 over the range $0.05 \lesssim k_1^* \lesssim 0.8$. As k_1^* approaches 1, noise becomes important (figure 4 shows that both $\phi_{\theta,1}$ and $\phi_{\theta,2}$ are affected) and the interpretation of $(\phi_{\theta,2})_{cal}/(\phi_{\theta,2})_{mea}$ becomes difficult since $(\phi_{\theta,2})_{cal}$ and $(\phi_{\theta,2})_{mea}$ are unlikely to be reliable. For $k_1^* \lesssim 0.8$, the trend of figure 11, which suggests greater anisotropy at $\xi = 0.53$ and 1.06 than at $\xi = 0$, should be reliable. (It is unlikely that this result is affected by the fact that isotropy has already been used for correcting the spectra since the use of uncorrected spectra leads to essentially the same result.) This trend may reflect the influence of the mean shear. A suitable measure of the latter is given by the non-dimensional parameter $S\overline{q^2}/2\bar{\epsilon}$, where S is $|\partial\bar{U}/\partial x_2|$. In the present flow, this parameter increases from zero on the axis to a maximum of about 2.5 at $\xi \approx 1$. For comparison, the maximum values of $S\overline{q^2}/2\bar{\epsilon}$ in a plane jet and a plane wake are 2.8 and 3.0 respectively. The differences in the maximum values of $S\overline{q^2}/2\bar{\epsilon}$ in the three flows do not appear to be sufficiently important to explain the smaller anisotropy of the circular jet. Figure 10 shows that the departure from isotropy is not very different between $\xi = 0.53$ ($S\overline{q^2}/2\bar{\epsilon} \approx 2.0$) and $\xi = 1.06$ ($S\overline{q^2}/2\bar{\epsilon} \approx 2.5$).

The large-scale structures which make up the organized motion in the circular jet derive from a number of primary modes of instability of the flow. Each mode is likely to have coupled axial, radial and/or azimuthal components. The resulting complex three-dimensionality is observed in flow visualizations (e.g. Dimotakis, Miake-Lye & Papantoniou 1983 and Yoda, Hesselink & Mungal 1991). Using an array of eight X-probes and a time-delay probability method, Chua & Antonia (1992) noted the coexistence at $x_1/d = 10$ and $x_1/d = 15$ of both symmetrical and antisymmetrical

(possibly helical) modes. Yoda, Hesselink & Mungal (1992) concluded that the jet far-field has a tendency to switch between axisymmetric and helical modes. This inherent three-dimensionality seems a likely contributor to the relatively small departure from isotropy, at least in the context of equation (4), in the present flow. The plane jet and the plane wake have a lower number of primary instability modes which may result in an increased tendency to anisotropy.

8. Conclusions

Measurements of the three components of the average temperature dissipation have been determined in the self-preserving region of a turbulent round jet using a pair of parallel cold wires separated in either the streamwise, radial or azimuthal directions. Estimates of these components were made using the correlation method by first correcting the attenuation of the high-wavenumber part of the derivative spectra caused by the separation between wires. The two methods yield essentially the same results. The accuracy of the measured temperature dissipation was reflected in the plausible distribution of the turbulent diffusion term, which was obtained by difference from the budget of the temperature variance.

The variances of the radial and azimuthal temperature derivatives are approximately equal, their magnitude being only slightly larger than that of the streamwise derivative. Support for this result is provided by the general agreement between the measured transverse derivative spectra and those calculated from the streamwise derivative spectrum using isotropy. This agreement becomes less perfect away from the axis, reflecting the possible importance of the mean shear.

Comparison of the present results with those previously obtained in a plane jet and a plane wake indicates that local isotropy is a better approximation for the circular jet than for either of the other two flows. This appears to be associated with the more complex (three-dimensional) aspects of the organized motion of the circular jet. Although the temperature jumps make an important contribution to the temperature variance, their contribution to the temperature-derivative variances was found to be small.

The support of the Australian Research Council is acknowledged.

Appendix

The temperature fluctuation at location x can be expressed using a Fourier–Stieltjes representation (e.g. Batchelor 1953; Lumley & Panofsky 1964)

$$\theta(\boldsymbol{x}) = \int_{-\infty}^{\infty} \mathrm{e}^{\mathrm{j}\boldsymbol{k}\cdot\boldsymbol{x}}\,\mathrm{d}Z_\theta(\boldsymbol{k}) \tag{A 1}$$

where $\mathrm{j} = \sqrt{-1}$, $\boldsymbol{k}$ is the wavenumber vector and $\mathrm{d}Z_\theta(\boldsymbol{k})$ is the Fourier coefficient corresponding to the wavenumber vector $\boldsymbol{k}$. The derivative $\theta_{,i}$ follows directly from (A 1), namely

$$\theta_{,i}(\boldsymbol{x}) = \mathrm{j}\int_{-\infty}^{\infty} k_i\,\mathrm{e}^{\mathrm{j}\boldsymbol{k}\cdot\boldsymbol{x}}\,\mathrm{d}Z_\theta(\boldsymbol{k}). \tag{A 2}$$

The corresponding one-dimensional spectrum is

$$\phi_{\theta_{,i}}(k_1) = \iint_{-\infty}^{\infty} k_i^2\,\phi(\boldsymbol{k})\,\mathrm{d}k_2\,\mathrm{d}k_3 \tag{A 3}$$

where $\phi(k)\,\mathrm{d}k \equiv \mathrm{d}Z_\theta(k)\,\mathrm{d}Z_\theta^*(k)$ (the asterisk denotes the complex conjugate) is the three-dimensional temperature spectral density. The modification to (A 3) which results from the effect of the separation Δx_i may be written

$$\phi_{\theta,i}(k_1, \Delta x_i) = \frac{4}{(\Delta x_i)^2} \int\int_{-\infty}^{\infty} \sin^2(\tfrac{1}{2}k_i \Delta x_i)\, \phi(k)\, \mathrm{d}k_2\, \mathrm{d}k_3. \tag{A 4}$$

The above relations are valid for homogeneous turbulence; under the more restrictive assumption of isotropy, (A 4) can be rewritten as (6) in §4.

REFERENCES

ANSELMET, F., ANTONIA, R. A., BENABID, T. & FULACHIER, L. 1990 Effect of wall suction on the transport of a scalar by coherent structures in a turbulent boundary layer. In *Structure of Turbulence and Drag Reduction* (ed. A. Gyr), pp. 349–356. Springer.

ANTONIA, R. A., ANSELMET, F. & CHAMBERS, A. J. 1986 Assessment of local isotropy using measurements in a turbulent plane jet. *J. Fluid Mech.* **163**, 365–391.

ANTONIA, R. A. & BROWNE, L. W. B. 1983 The destruction of temperature fluctuations in a turbulent plane jet. *J. Fluid Mech.* **134**, 67–83.

ANTONIA, R. A. & BROWNE, L. W. B. 1986 Anisotropy of the temperature dissipation in a turbulent wake. *J. Fluid Mech.* **163**, 393–403.

ANTONIA, R. A., BROWNE, L. W. B. & CHAMBERS, A. J. 1981 Determination of time constants of cold wires. *Rev. Sci. Instrum.* **52**, 1382–1385.

ANTONIA, R. A., BROWNE, L. W. B. & CHAMBERS, A. J. 1985 Relations between spectra of spatial derivatives of temperature in a turbulent jet. *Phys. Fluids* **28**, 420–423.

ANTONIA, R. A., BROWNE, L. W. B., RAJAGOPALAN, S. & CHAMBERS, A. J. 1983 On the organized motion of a turbulent plane jet. *J. Fluid Mech.* **134**, 49–66.

ANTONIA, R. A., CHAMBERS, A. J., BRITZ, D. & BROWNE, L. W. B. 1986 Organized structures in a turbulent plane jet: topology and contribution to momentum and heat transport. *J. Fluid Mech.* **172**, 211–229.

ANTONIA, R. A., CHAMBERS, A. J. & HUSSAIN, A. K. M. F. 1980 Errors in simultaneous measurements of temperature and velocity in the outer part of a heated jet. *Phys. Fluids* **23**, 871–874.

ANTONIA, R. A. & FULACHIER, L. 1989 Topology of a turbulent boundary layer with and without wall suction. *J. Fluid Mech.* **198**, 429–451.

ANTONIA, R. A., KIM, J. & BROWNE, L. W. B. 1991 Some characteristics of small-scale turbulence in a turbulent duct flow. *J. Fluid Mech.* **233**, 369–388.

ANTONIA, R. A. & MI, J. 1993 Corrections for velocity and temperature derivatives in turbulent flows. *Expts. Fluids* (to appear).

ANTONIA, R. A., PRABHU, A. & STEPHENSON, S. E. 1975 Conditionally sampled measurements in a heated turbulent jet. *J. Fluid Mech.* **72**, 455–480.

BATCHELOR, G. K. 1953 *The Theory of Homogeneous Turbulence.* Cambridge University Press.

BILGER, R. W. 1989 Turbulent Diffusion Flames. *Ann. Rev. Fluid Mech.* **21**, 101–135.

BISSET, D. K., ANTONIA, R. A. & BROWNE, L. W. B. 1990 Spatial organization of large structures in the turbulent far wake of a cylinder. *J. Fluid Mech.* **218**, 439–461.

BROADWELL, J. E. & MUNGAL, M. G. 1991 Large-scale structures and molecular mixing. *Phys. Fluids* A **3**, 1193–1206.

BROWNE, L. W. B., ANTONIA, R. A. & CHAMBERS, A. J. 1983*a* Effect of the separation between cold wires on the spatial derivatives of temperature in a turbulent flow. *Boundary-Layer Met.* **27**, 129–139.

BROWNE, L. W. B., ANTONIA, R. A. & RAJAGOPALAN, S. 1983*b* The spatial derivative of temperature in a turbulent flow and Taylor's hypothesis. *Phys. Fluids* **26**, 1222–1227.

BROWNE, L. W. B., ANTONIA, R. A. & SHAH, D. A. 1987 Turbulent energy dissipation in a wake. *J. Fluid Mech.* **179**, 307–326.

CERVANTES DE GORTARI, J. & GOLDSCHMIDT, V. W. 1981 The apparent flapping motion of a turbulent plane jet – further experimental results. *Trans. ASME* I: *J. Fluids Engng* **103**, 119–126.

CHAMPAGNE, F. H., HARRIS, V. G. & CORRSIN, S. 1970 Experiments on nearly homogeneous turbulent shear flow. *J. Fluid Mech.* **41**, 81–139.

CHUA, L. P. 1989 Measurements in a turbulent circular jet PhD thesis, University of Newcastle, Australia.

CHUA, L. P. & ANTONIA, R. A. 1986 The turbulent interaction region of a circular jet. *Intl Commun. Heat Mass Transfer* **13**, 545–558.

CHUA, L. P. & ANTONIA, R. A. 1990 Turbulent Prandtl number in a circular jet. *Intl J. Heat Mass Transfer* **33**, 331–339.

CHUA, L. P. & ANTONIA, R. A. 1992 Spatial organization of large structures in the near-field of a circular jet. *Fluid Dyn. Res.* **9**, 59–71.

DIMOTAKIS, P. E., MIAKE-LYE, R. C. & PAPANTONIOU, D. A. 1983 Structure and dynamics of round turbulent jets. *Phys. Fluids* **26**, 3185–3192.

GEORGE, W. K. & HUSSEIN, H. J. 1991 Locally axisymmetric turbulence. *J. Fluid Mech.* **233**, 1–23.

GEORGE, W. K., HUSSEIN, H. J. & WOODWARD, S. H. 1989 An evaluation of the effect of a fluctuating convection velocity on the validity of Taylor's hypothesis. In *Proc. Tenth Australasian Fluid Mechanics Conference, Melbourne*, pp. 11.5–11.8.

HUSSEIN, H. J. 1988 Measurement of small scale turbulence in an axisymmetric jet using moving hot wires. *Tech. Rep.* 121, Turbulence Research Laboratory, State University of New York at Buffalo.

HUSSEIN, H. J. & GEORGE, W. K. 1989 Measurement of small scale turbulence in an axisymmetric jet using moving hot-wires. In *Proc. 7th Symp. on Turbulent Shear Flows, Stanford University*, pp. 30.21–30.26.

KLEWICKI, J. C. & FALCO, R. E. 1990 On accurately measuring statistics associated with small-scale structure in turbulent boundary layers using hot-wire probes. *J. Fluid Mech.* **219**, 119–142.

KRISHNAMOORTHY, L. V. & ANTONIA, R. A. 1987 Temperature dissipation measurements in a turbulent boundary layer. *J. Fluid Mech.* **176**, 265–281.

LOCKWOOD, F. C. & MONEIB, H. A. 1980 Fluctuating temperature measurements in a heated round free jet. *Combust. Sci. Tech.* **22**, 63–81.

LUMLEY, J. L. 1965 Interpretation of time spectra measured in high-intensity shear flows. *Phys. Fluids* **8**, 1056–1062.

LUMLEY, J. L. & PANOFSKY, H. A. 1964 *The Structure of Atmospheric Turbulence*. Interscience.

MESTAYER, P. 1982 Local isotropy and anisotropy in a high-Reynolds-number turbulent boundary layer. *J. Fluid Mech.* **125**, 475–503.

MESTAYER, P. & CHAMBAUD, P. 1979 Some limitations to measurements of turbulence microstructure with hot and cold wires. *Boundary-Layer Met.* **16**, 311–329.

MONIN, A. S. & YAGLOM, A. M. 1975 *Statistical Fluid Mechanics*, Vol. 2. MIT Press.

NAGANO, Y. & KIM, C. 1988 A two-equation model for heat transport in wall turbulent shear flows. *Trans. ASME* C: *J. Heat Transfer* **110**, 583–589.

NAMAZIAN, M., SCHEFER, R. W. & KELLY, J. 1988 Scalar dissipation measurements in the developing region of a jet. *Combust. Flame* **74**, 147–160.

PARANTHOEN, P., PETIT, C. & LECORDIER, J. C. 1982 The effect of thermal prong–wire interaction on the response of a cold wire in gaseous flows (air, argon and helium). *J. Fluid Mech.* **124**, 457–473.

ROSE, W. G. 1966 Results of an attempt to generate a homogeneous turbulent shear flow. *J. Fluid Mech.* **25**, 97–120.

SREENIVASAN, K. R. 1991 On local isotropy of passive scalars in turbulent shear flows. *Proc. R. Soc. Lond.* A **434**, 165–182.

SREENIVASAN, K. R., ANTONIA, R. A. & BRITZ, D. 1979 Local isotropy and large structures in a heated turbulent jet. *J. Fluid Mech.* **94**, 745–775.

SREENIVASAN, K. R., ANTONIA, R. A. & DANH, H. Q. 1977 Temperature dissipation fluctuations in a turbulent boundary layer. *Phys. Fluids* **20**, 1238–1249.

TAVOULARIS, S. & CORRSIN, S. 1981 Experiments in nearly homogeneous turbulent shear flow with a uniform mean temperature gradient. Part 1. *J. Fluid Mech.* **104**, 311–347.

TOWNSEND, A. A. 1956 *The Structure of Turbulent Shear Flow*, Cambridge University Press.

TSO, J., KOVASZNAY, L. S. G. & HUSSAIN, A. K. M. F. 1981 Search for large-scale coherent structure in the nearly self-preserving region of a turbulent axisymmetric jet. *Trans. ASME* I: *J. Fluids Engng* **103**, 503–508.

TULAPURKARA, E. G., ANTONIA, R. A. & BROWNE, L. W. B. 1989 Optimisation of a $\overline{\theta^2} - \epsilon_\theta$ model for a turbulent far wake. In *Proc. Seventh Symp. on Turbulent Shear Flows, Stanford*, pp. 29.2.1–29.2.6.

VAN ATTA, C. W. 1977 Second-order spectral local isotropy in turbulent scalar fields. *J. Fluid Mech.* **80**, 609–615.

VAN CRUYNINGEN, I., LOZANO, A. & HANSON, R. K. 1990 Quantitative imaging of concentration by planar laser-induced fluorescence. *Expts. Fluids* **10**, 41–49.

VEROLLET, E. 1972 Etude d'une couche limite turbulence avec aspiration et chauffage à la paroi. Thèse Doctorat ès Sciences, Université d'Aix-Marseille (also *Rapport* CEA-4872, 1977).

WYGNANSKI, I. & FIEDLER, H. 1969 Some measurements in the self-preserving jet. *J. Fluid Mech.* **38**, 577–612.

WYNGAARD, J. C. 1968 Measurement of small scale turbulence structure with hot wires. *J. Sci. Instrum.* **1**, 1105–1108.

WYNGAARD, J. C. 1971 Spatial resolution of a resistance wire temperature sensor. *Phys. Fluids* **4**, 2052–2054.

WYNGAARD, J. C. & CLIFFORD, S. F. 1977 Taylor's hypothesis and high-frequency turbulence spectra. *J. Atmos. Sci.* **34**, 922–929.

YODA, M., HESSELINK, L. & MUNGAL, M. G. 1991 The temporal evolution of large-scale structures in the turbulent jet. *Proc. Eighth Symp. on Turbulent Shear Flows*, pp. 6-1-1–6-1-6.

YODA, M., HESSELINK, L. & MUNGAL, M. G. 1992 The evolution and nature of large-scale structures in the turbulent jet. *Phys. Fluids* A **4**, 803–811.